EurJOC
European Journal of Organic Chemistry

Full Papers
doi.org/10.1002/ejoc.202001420

Chemistry Europe
European Chemical Societies Publishing

Special Collection

Synthesis, Self-Assembly, and Nucleic Acid Recognition of an Acylhydrazone-Conjugated Cationic Tetraphenylethene Ligand

Maëva Coste,[a] Clément Kotras,[b, c] Yannick Bessin,[a] Virginie Gervais,[d] David Dellemme,[c] Maxime Leclercq,[c] Mathieu Fosséprè,[c] Sébastien Richeter,[b] Sébastien Clément,*[b] Mathieu Surin,*[c] and Sébastien Ulrich*[a]

Supramolecular polymers are of interest in the pursuit of multivalent nucleic acids recognition. However, their formation often relies on non-covalent forces that are also at play in the interaction with nucleic acids. In this work, we designed a novel compound (**TPE-Gir**) combining a tetraphenylethene aromatic core tethered to four quaternary ammoniums through acylhydrazone spacers, and we investigated in detail its self-assembly and interaction with different types of nucleic acids. The spectroscopic analyses indicate the self-assembly of regular fluorescent nanoparticles (observed by DLS and TEM) in the absence of nucleic acids, the strong propensity to intercalate into single-stranded DNA, the ability to bind into the minor groove of double-stranded DNA, and the selective binding to G-quadruplex (G4) structures by fitting within a wide G4-groove. Those recognition events are quantified by isothermal titration calorimetry and the proposed binding models are supported by docking simulations.

Introduction

Supramolecular polymers are formed through the non-covalent association of monomers. An important class of supramolecular polymers features monomers, such as benzene-1,3,5-triscarboxamides (BTAs), that associate through a combination of π-stacking interactions and hydrogen bonds into 1D rod-like supramolecular polymers in a cooperative fashion.[1] However, the design may be particularly sensitive to the molecular structure and minute changes have been reported to greatly impact the nature of the resulting supramolecular polymers as well as their mechanisms of formation.[1–2] These materials have attracted great interest in materials science for their dynamic self-healing properties,[3] and have recently been considered for their potential application in life sciences.[4] In particular, the dynamic expression of multivalency through controlled self-assembly and disassembly processes is an effective way toward smart biorecognition and delivery.

The recognition and delivery of nucleic acids requires multivalent binding which may be achieved using supramolecular polymers.[5] However, interfacing supramolecular polymerization with DNA recognition is not straightforward since nucleic acids recognition involves multiple non-covalent forces (*e.g.* π-stacking, hydrogen bonds, electrostatic interactions) that may compete with the formation of supramolecular polymers. Thus, if the non-covalent interactions between aromatic monomers and the nucleic acids dominate, then those aromatic compounds can individually bind and self-organize onto nucleic acid templates, for instance through groove binding or intercalation through base pairs,[6] as it is the case for cyanine and proflavine derivatives (Figure 1A).[6b–e] Alternatively, if the supramolecular polymer is robust to the presence of nucleic acid, a multivalent binding may happen, either through a programmed polymerization that take place prior to nucleic acid binding,[4b,7] or in a nucleic acid-templated manner when supramolecular polymerization is triggered upon nucleic acid binding (Figure 1A).[8] Examples of the latter case have been reported that involve the self-assembly, by π-π stacking of π-conjugated compounds into supramolecular polymers (*e.g.* benzene[9]/naphthalene[10]/pyrene,[11] porphyrins,[12] corroles,[13] perylene diimides,[14] triarylamines,[15] and oligo(*p*-phenylene vinylene)[16]).[5] The divide between those modes of self-assembly rests on a delicate balance of forces (ligand-ligand interactions *vs.* ligand-DNA interactions) that still remain difficult to anticipate. Programmed self-assembly occurs when ligand-ligand interactions dominate whereas effective templated self-

[a] *M. Coste, Y. Bessin, Dr. S. Ulrich*
IBMM, Université de Montpellier, CNRS, ENSCM,
Montpellier, France
E-mail: sebastien.ulrich@enscm.fr
https://ibmm.umontpellier.fr/spip.php?page=pageperso&id_user=434
[b] *Dr. C. Kotras, Dr. S. Richeter, Prof. S. Clément*
ICGM Institut Charles Gerhardt Montpellier, UMR 5253, Université de Montpellier,
CNRS, ENSCM,
Montpellier, France
E-mail: sebastien.clement1@umontpellier.fr
https://www.icgm.fr/sebastien-clement
[c] *Dr. C. Kotras, D. Dellemme, M. Leclercq, Dr. M. Fosséprè, Dr. M. Surin*
Laboratory for Chemistry of Novel Materials,
Center of Innovation and Research in Materials and Polymers (CIRMAP),
University of Mons-UMONS,
7000 Mons, Belgium
E-mail: mathieu.surin@umons.ac.be
http://morris.umons.ac.be/bio-inspired-chemistry/
[d] *Dr. V. Gervais*
CNRS, Institut de Pharmacologie et de Biologie Structurale (IPBS),
Université de Toulouse, UPS,
205 route de Narbonne, 31077 Toulouse, France

Supporting information for this article is available on the WWW under https://doi.org/10.1002/ejoc.202001420

Part of the "YourJOC Talents" Special Collection.

Maëva Coste carried out a bachelor degree in organic chemistry at the University of Montpellier, France. Then, she pursued and obtained a Master degree in chemistry of biomolecules in 2018. She is currently doing her PhD in biomolecular engineering at the University of Montpellier, in the Institut des Biomolécules Max Mousseron (IBMM), under the supervision of Dr. Sébastien Ulrich. Her thesis projects are focused on the design, synthesis and characterization of programmed and DNA-templated self-assemblies of aromatic conjugates.

Clément Kotras is a Ph.D. graduate from UMontpellier (France) and UMons (Belgium) since 2019. He obtained a Master degree in Chemistry (Applied Synthesis, Separation, and Analysis) from the Université de Montpellier (France) in 2016. His Master thesis was about the optimization of the synthesis of sugar-phosphate derivative. In 2016, he started a joint PhD between the Laboratory for Chemistry of Novel Materials at UMons and the laboratory of Chimie Macromoléculaire et Organisation du Solide at UMontpellier, under the supervision of Pr. Mathieu Surin and Pr. Sébastien Clément. His PhD research topic deals with π-conjugated materials for applications in health, through the design and spectroscopic characterization of small molecular probes and dynamic polymers that bind DNA.

Yannick Bessin obtained his PhD in cellular biochemistry from the University of Rouen in 2004. Thereafter, he was recruited as a CNRS engineer to set up a protein production and purification platform at the Centre de Biologie Structurale (CBS) in Montpellier, which he was in charge of for 8 years. In 2012 he joined the group of Pascal Dumy at the Institut des Biomolécules Max Mousseron (IBMM) in Montpellier to provide his expertise in protein purification, biochemistry and enzyme assays. He works on projects involving peptide synthesis, nucleic acids recognition and delivery, and enzyme inhibition assays.

Virginie Gervais obtained her PhD in Molecular Biophysics at the Pierre et Marie Curie University (Paris). After graduation, she spent 3 years at EMBL (Heidelberg, Germany) and 3 years at ESBS (Illkirch, France) for postdoctoral studies under the supervision of Prof. H. Oschkinat and Prof. B. Kieffer, respectively. She then moved to IPBS (Toulouse, France) and joined the team of Prof. A. Milon in 2002 as a CNRS researcher. Her main research interest focuses on structural and thermodynamic studies of protein-DNA complexes using high-resolution NMR and ITC.

David Dellemme is currently completing his master thesis (2021) at the University of Mons-UMONS, Belgium. Within the laboratory for Chemistry of Novel Materials, his research deals with the study of sequence-defined oligomers. His main interests are related to bioinspired chemistry.

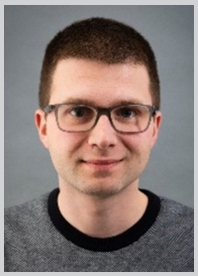

Maxime Leclercq received a master degree in Chemical Sciences from the University of Mons in 2017. The same year he joined the laboratory for Chemistry of Novel Materials as a PhD student in the group of Prof. Roberto Lazzaroni, under the supervision of Prof. Mathieu Surin. His research topic is to develop of DNA/π-conjugated polymers supramolecular assemblies for biosensing, in particular for the detection of specific DNA and for probing methylation by enzymes.

Mathieu Fossépré received his PhD in Chemistry under the supervision of Prof. Daniel P. Vercauteren (University of Namur, Belgium) and Prof. Aatto Laaksonen (Stockholm University, Sweden). His work aimed at describing throughout molecular simulations the flexibility of the μ opioid receptor. In 2016, he joined the University of Mons as postdoctoral fellow to study bioinspired materials with Prof. Mathieu Surin. Since 2018, he is involved in the design of sequence-defined polymers for catalysis and biorecognition.

Sébastien Richeter completed his PhD in 2003 with Dr. H. J. Callot and Dr. R. Ruppert at the University of Strasbourg. After a postdocoral position in the research group of Prof. J. Rebek Jr. at the Scripps Research Institute (La Jolla, USA), he was appointed in 2004 as Lecturer at the University of Montpellier in France. His current research topics include porphyrins and other π-conjugated molecules for materials sciences, biomedical applications and catalysis.

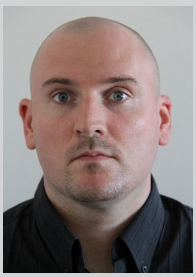

Sébastien Clément got his PhD in the University of Franche-Comté (France) in 2006 with Pr. M. Knorr and Dr. L. Guyard. After two post-doctoral trainings with Prof. P. D. Harvey at the University of Sherbrooke (Canada) and Prof. P. Dubois at the University of Mons (Belgium), he was appointed as Lecturer in 2009 and Professor in 2018 at the University of Montpellier (France). His current research interests are the study of π-conjugated and hybrid materials for applications ranging from biosensing and therapy to solar energy conversion.

Mathieu Surin is senior research associate FNRS, Belgium. Since 2009, he has developed a research line on DNA-based supramolecular assemblies. In 2015, he was invited professor at the University of Montpellier. Since 2017, he is associate professor at the University of Mons—UMONS, where he leads a research team in the field of Bioinspired Chemistry. His current research interests are DNA recognition and detection, and nanomaterials inspired by biopolymers.

Sébastien Ulrich carried out his PhD with Prof. Jean-Marie Lehn (Université de Strasbourg, France), and post-docs with Prof. Harry L. Anderson (Oxford University, UK) and Prof. Eric T. Kool (Stanford University, CA, USA). In 2011, he was awarded an ANR starting grant and joined the group of Prof. Pascal Dumy in Grenoble, before moving in 2012 to Montpellier, France where he was recruited by the CNRS to develop his research interests in the field of supramolecular bioorganic chemistry. Since then, he has contributed to developing dynamic self-assemblies for nucleic acid recognition and delivery applications. In 2017, he was awarded the CNRS Bronze Medal.

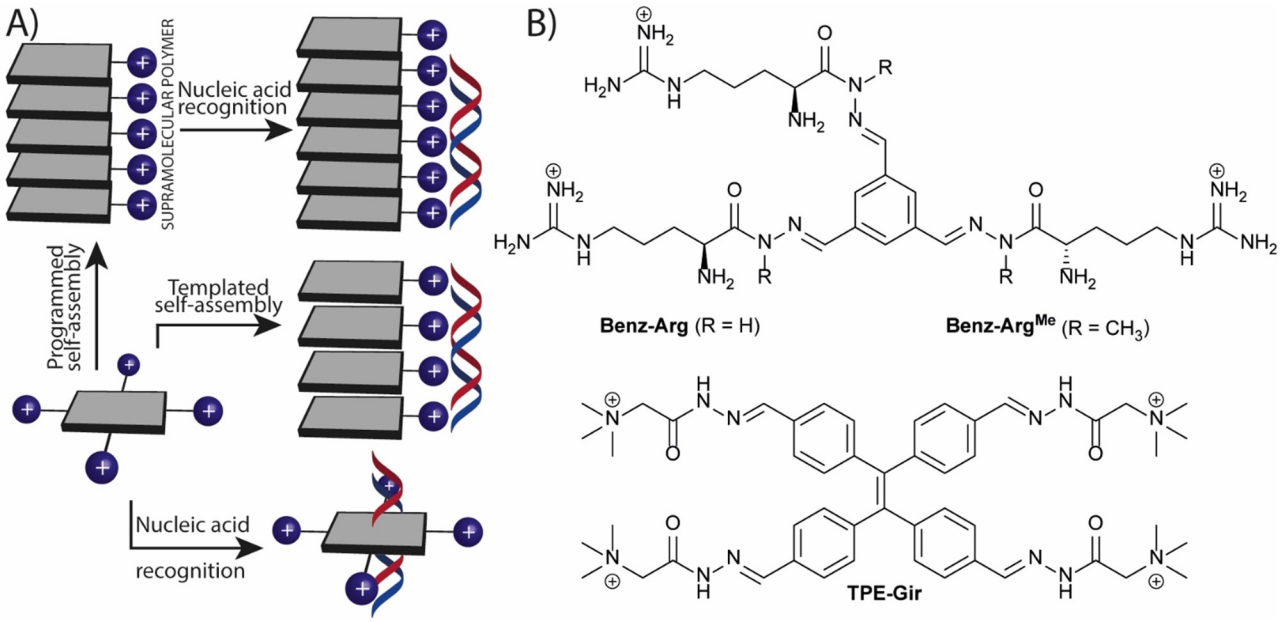

Figure 1. A) Sketch of the possible modes of self-assembly of cationic aromatics: nucleic acid recognition of individual compounds through groove binding or base pair intercalation, templated self-assembly assisted by π-π stacking, and programmed self-assembly of supramolecular polymers that recognize nucleic acids through multivalent interactions; B) Chemical structures of DNA-binding ligands made of different aromatic cores coupled to cationic moieties through acylhydrazone ligations. Counterions (Cl^-) are omitted for clarity.

assembly requires both strong ligand-ligand and strong ligand-DNA interactions.[17] In this case, having secondary interactions such as π-π interactions between aromatic ligands can help strengthen ligand-ligand interactions.

In this context, compounds that feature a central aromatic π-conjugated core functionalized with cationic head groups through acylhydrazone linkages that can potentially give rise to intermolecular hydrogen bonds similarly to BTAs are of particular interest. We found effective DNA binding using **Benz-Arg** (Figure 1B), which was quite surprising and unexpected given the low valency of these compounds (6 positive charges from 3 guanidinium and 3 ammonium groups) and the lack of pre-organization (the 3 cationic moieties being flexible and probably not oriented toward the same direction).[18] Thus, we suspected that a self-assembly process may take place and account for the observed activity. In this work, we question the mode of self-assembly, whether these compounds lead to programmed or DNA-templated supramolecular polymers, or whether an alternative binding process takes place (see sketch Figure 1A). In a prior work, we set up on probing the role of hydrogen bonds which could be involved in BTAs-like supramolecular polymerization. However, gel electrophoresis and ethidium bromide displacement assay revealed no difference in DNA binding between **Benz-Arg** and its N-methylated version **Benz-Arg^{Me}** (Figure 1B) which can act as a chain-stopper for supramolecular polymers,[19] thereby ruling out the prime role of hydrogen bonds in this context.[20] We then turned our attention to extended aromatic cores which could display exalted π-stacking interactions or hydrophobic interactions, and tetraphenylethene (TPE) as π-conjugated core was selected. TPE derivatives are well-known for their aggregation-induced emission (AIE) which results in an unusual enhancement of fluorescence emission upon aggregation.[21] TPEs are therefore attractive candidates as turn-on fluorescent (bio)probes[22] and supramolecular polymers incorporating TPE have thus been made.[23] Besides, various TPE derivatives functionalized with cationic moieties, have been reported for the recognition of single-stranded (ss) DNA,[24] double-stranded (ds) DNA,[24–25] and DNA G-quadruplexes.[26] While the nature of the pendant cationic groups (*e.g.* primary ammonium *vs.* quaternary ammonium) as well as the structure of the aromatic TPE core (*E* vs. *Z* isomers) and thus the spatial presentation of those cationic groups have been found to play an important role on the binding affinity and selectivity,[24] the role of self-assembly and the binding mode to DNA remain unclear. Herein, we report the design, synthesis, self-assembly and interaction with different types of DNA (ssDNA, dsDNA, and G-quadruplex) of compound **TPE-Gir** (Figure 1) that combines a TPE aromatic core, terminal quaternary ammonium groups for DNA binding through electrostatic interactions, and acylhydrazone spacers that can potentially form hydrogen bonds.

Results and Discussion

Design and synthesis. The design of **TPE-Gir** is based on a versatile click functionalization of a tetraphenylethene. We have recently described a TPE grafted with four aldehyde groups that can undergo subsequent acylhydrazone conjugation reaction.[27] The acylhydrazone motif is indeed interesting for its well-known potential to engage in hydrogen bond interactions which often play a key role in supramolecular polymerization.[28]

TPE-Gir was synthesized using acylhydrazone ligation reactions by reacting the tetraaldehyde **TPE-Ald**[27] with an excess (2 eq. per aldehyde) of the commercially-available Girard's reagent T (Scheme 1) in refluxing ethanol. The desired water-soluble **TPE-Gir** was isolated by reverse-phase HPLC in 71% yield and characterized by NMR spectroscopy and mass spectrometry. The compound presents itself as an inseparable mixture of two isomers in a 7:3 ratio, assigned to *E*/*Z* acylhydrazone isomers since the largest difference in chemical shift is seen for the imine proton (Figure S2).

Self-assembly of TPE-Gir. We first studied the self-assembly properties of **TPE-Gir. TPE-Gir** appears molecularly-dissolved in aqueous buffer, probably due to repulsive electrostatic forces between the quaternary ammonium groups, whereas addition of a non-solvent such as THF leads to aggregation. This was evidenced by TEM analysis showing only few aggregates in 100% water, whereas numerous spherical objects with diameters centered around 100 nm are clearly seen in THF/H_2O 99/1 (v/v) (Figure 2A). DLS analysis provides a qualitative and quantitative confirmation, yielding Z-average diameters of 120 nm with a narrow polydispersity index of 0.14 (Figure 2B). In comparison, previous reports on different cationic TPE derivatives reported the formation of spherical objects with sizes ranging from 20 to 500 nm.[29] Further spectroscopic analyses reveal hypo- and batho-chromic shifts in the electronic absorption spectra, respectively at 310 nm and 430 nm, upon addition of THF – the effects being marked beyond 90% THF (Figure 2C). The red-shift (430 nm) can be attributed to an extended conjugation, endowed by an enforced coplanarity of the acylhydrazone moieties with the central TPE core. Interestingly, fluorescence emission at 510 nm was found to be concomitantly increased 35-fold upon aggregation (Figure 2D). These results show that AIE operates on **TPE-Gir** thanks to the presence of a non-solvent triggering aggregation. However, unlike supramolecular polymers such as BTAs, in this case we did not evidence the formation of linear fibers but instead closed spherical structures, most likely vesicles due to the bola-amphiphilic character of **TPE-Gir**.[30] The formation of such discrete objects may be the result of the frustrated growth of **TPE-Gir** which is favored by π-π stacking interactions or hydrophobic effect and disfavored by electrostatic repulsion.[31]

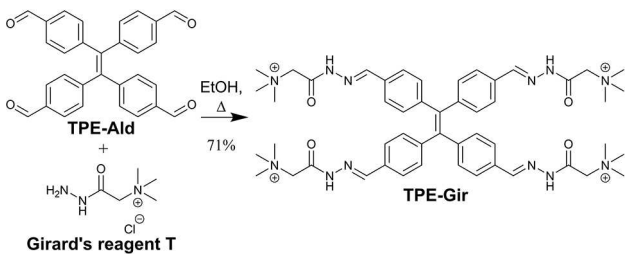

Scheme 1. Synthesis of **TPE-Gir** through acylhydrazone coupling reaction. Counterions (Cl^-) are omitted in the structure of **TPE-Gir**, for clarity.

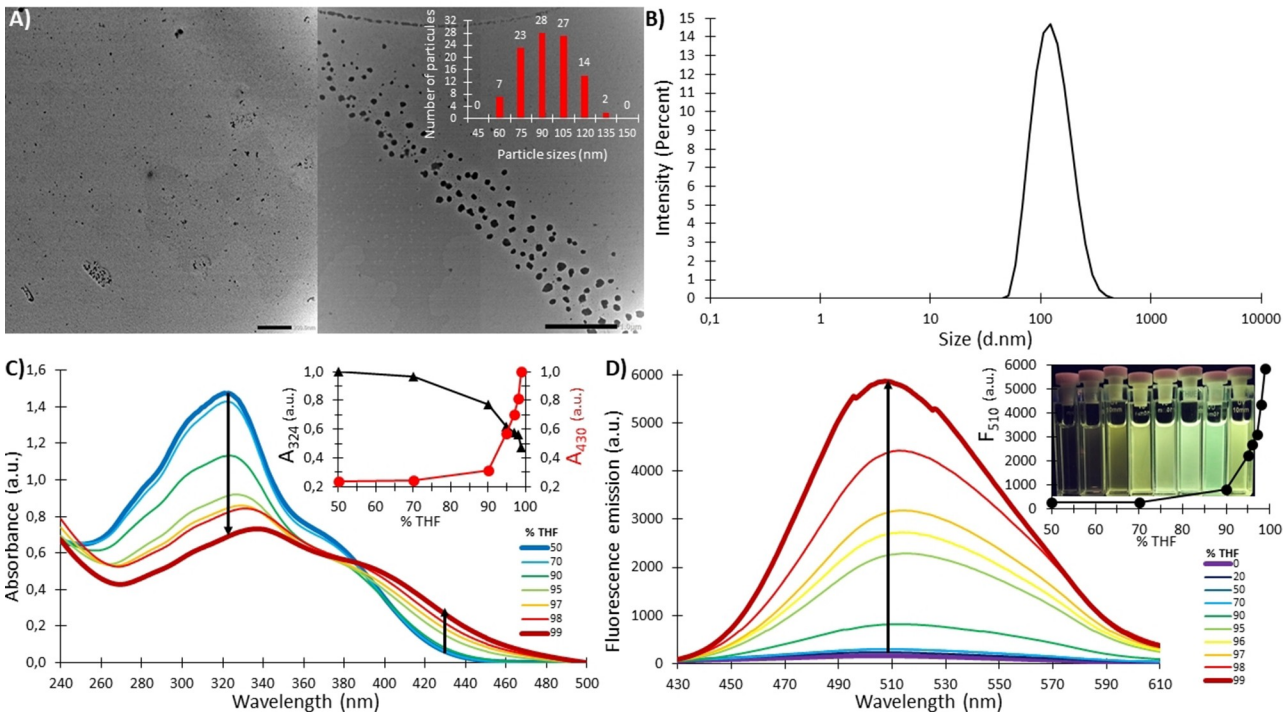

Figure 2. (A) TEM of **TPE-Gir** (0.025 mM) in 100% H_2O (left), in THF/H_2O 99/1 (right); (B) DLS analysis of **TPE-Gir** (0.025 mM) in THF/H_2O 99/1. HEPES buffer: 10 mM HEPES, 9.4 mM NaCl, 10 μM EDTA, pH 7.2; (C) UV-Visible absorption spectra of **TPE-Gir** (0.02 mM) in different THF/ HEPES (v/v) mixtures. **Inset**: Normalized evolution of **TPE-Gir** absorbances at 324 and 430 nm; (D) Fluorescence emission spectra of **TPE-Gir** (0.02 mM) in different THF/ HEPES (v/v) mixtures (λ_{exc} = 310 nm). **Inset**: Fluorescence emission evolution of **TPE-Gir** at λ_{em} = 510 nm; **Photograph**: Samples at increasing THF/H_2O ratios (from left to right) under light irradiation (310 nm).

Interaction with single-stranded DNA. Single-stranded DNA serves as a popular template to organize small aromatic molecules into chiral nanostructures through electrostatic interactions with the phosphodiester backbone (outside binding) or hydrogen bonds with nucleobases.[5,32] Although ssDNA is far less rigid than its double-stranded counterpart and best represented by a worm-like model, it keeps a helical structure with a persistence length that greatly increases under low salinity conditions (around 20 Å below 10 mM NaCl).[33] Since **TPE-Gir** appears molecularly-dissolved in aqueous buffer, we envisaged that attractive electrostatic interactions by formation of ion pairs with phosphodiesters of ssDNA would favor their subsequent ssDNA-templated supramolecular polymerization.[9,15,34]

UV-Vis absorption spectroscopy of **TPE-Gir** shows continuous hypo- and batho-chromic shifts upon addition of single-stranded calf thymus DNA (ss-CT-DNA), while fluorescence emission shows a progressive increase of the main peak at 515 nm (Figure 3A and Figure 3B). Using an oligonucleotide template (dT_{40}), circular dichroism (CD) spectroscopy shows a bisignate signal with a zero-crossing at 247 nm, and a weak negative induced CD (ICD) signal at 310 nm appearing as more **TPE-Gir** is titrated onto the solution of dT_{40} (Figure 3C). The induced CD signal at 310 nm demonstrates that a close interaction takes place between dT_{40} and **TPE-Gir**, leading to a transfer of chirality from the chiral ssDNA template to the achiral ligand. Job plot analysis obtained through fluorescence titration experiments shows that a maximum is reached at a stoichiometry around 1 ligand per 3 nucleobases (Figure 3D).

Therefore, **TPE-Gir** binding to DNA manifests through hypochromism and a shift to longer wavelength in the absorption spectra of the bound ligand,[35] along with a weak negative ICD signal, suggesting binding through intercalation.[36] A partial "intercalation-like" complex[37] could be evoked where the TPE core would stack between nucleobases while the quaternary ammonium group would interact through electrostatic interaction with the DNA phosphodiester backbone.[38] Thus, the enhancement in fluorescence emission is better explained by the restriction of intramolecular rotation due to intercalation within nucleobases rather than an effect promoted by aggregation.[39] Given the larger surface of **TPE-Gir** compared to nucleobases, we wondered whether such partial "intercalation-like" complex could leave room to the assembly of multiple ssDNA. Indeed, the observed binding stoichiometry of 1 ligand per 3 nucleobases has not reached the maximal value dictated by the nearest neighbor site exclusion principle[40] of 1 ligand per 2 nucleobases (Figure 4A). Alternatively, such binding stoichiometry could potentially fit a binding model involving two ssDNA strands, thus giving a stoichiometry of 1 ligand per 4 nucleobases (i.e. 2 pseudo base pairs) (Figure 4B). In order to probe the existence of such binding, we used (5′-FAM)-dT_{40} and dT_{40}-(3′-TAMRA) as fluores-

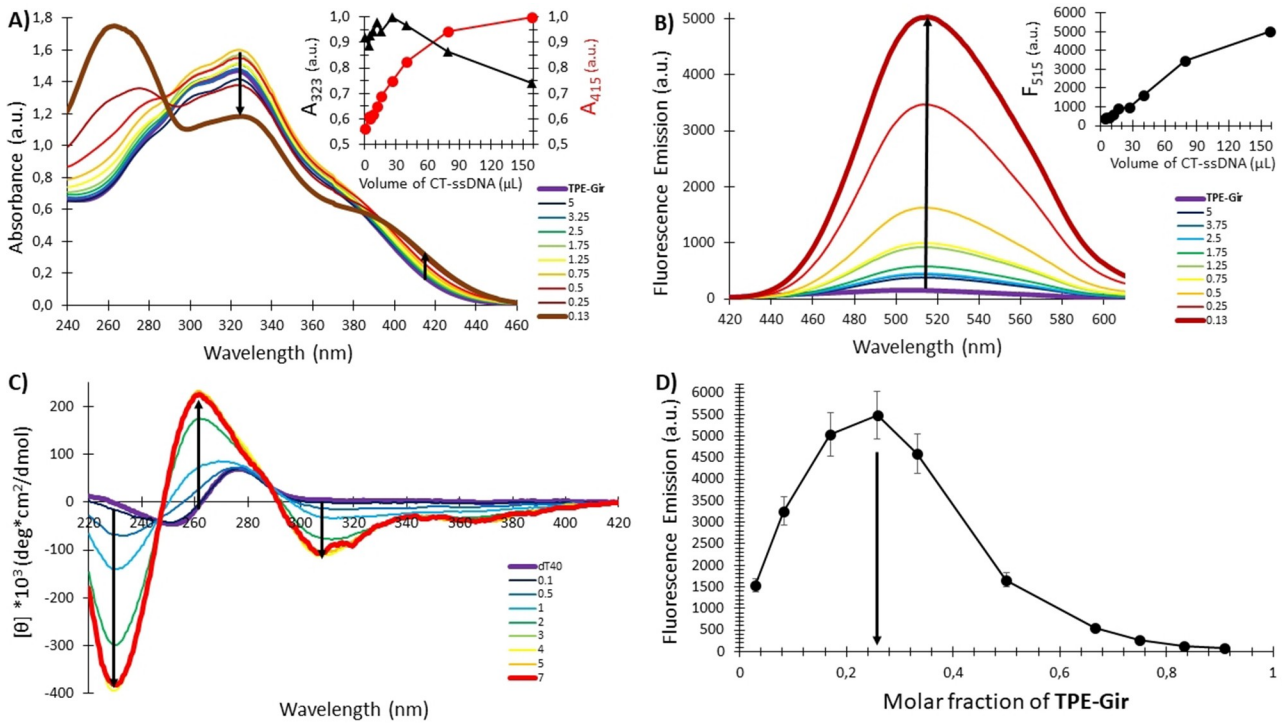

Figure 3. (A) UV-Visible titration of **TPE-Gir** (0.02 mM in HEPES) by ssCT-DNA at different molar ratios (final concentrations of 0.2 nM to 8 nM). **Inset**: Normalized evolution of **TPE-Gir**:ssCT-DNA absorbances at different volumes of ssCT-DNA (λ_{abs} = 323 and 415 nm); (B) Fluorescence emission spectra of **TPE-Gir** (0.02 mM in HEPES) by ssCT-DNA at different molar ratios (final concentrations of 0.2 nM to 8 nM) (λ_{exc} = 310 nm). **Inset**: Fluorescent emission evolution of **TPE-Gir**:ssCT-DNA spectra at different volumes of ssCT-DNA (λ_{em} = 515 nm); (C) CD titration of dT_{40} (final concentration of 13 µM in water) by **TPE-Gir** at different molar ratios in H_2O (final concentration of **TPE-Gir** of 0.012 mM to 0.6 mM); (D) Job plot obtained through fluorescence titration experiments (relative error of 10% applied). The molar ratios are expressed in ligand per nucleobase. HEPES buffer: 10 mM HEPES, 9.4 mM NaCl, 10 µM EDTA, pH 7.2.

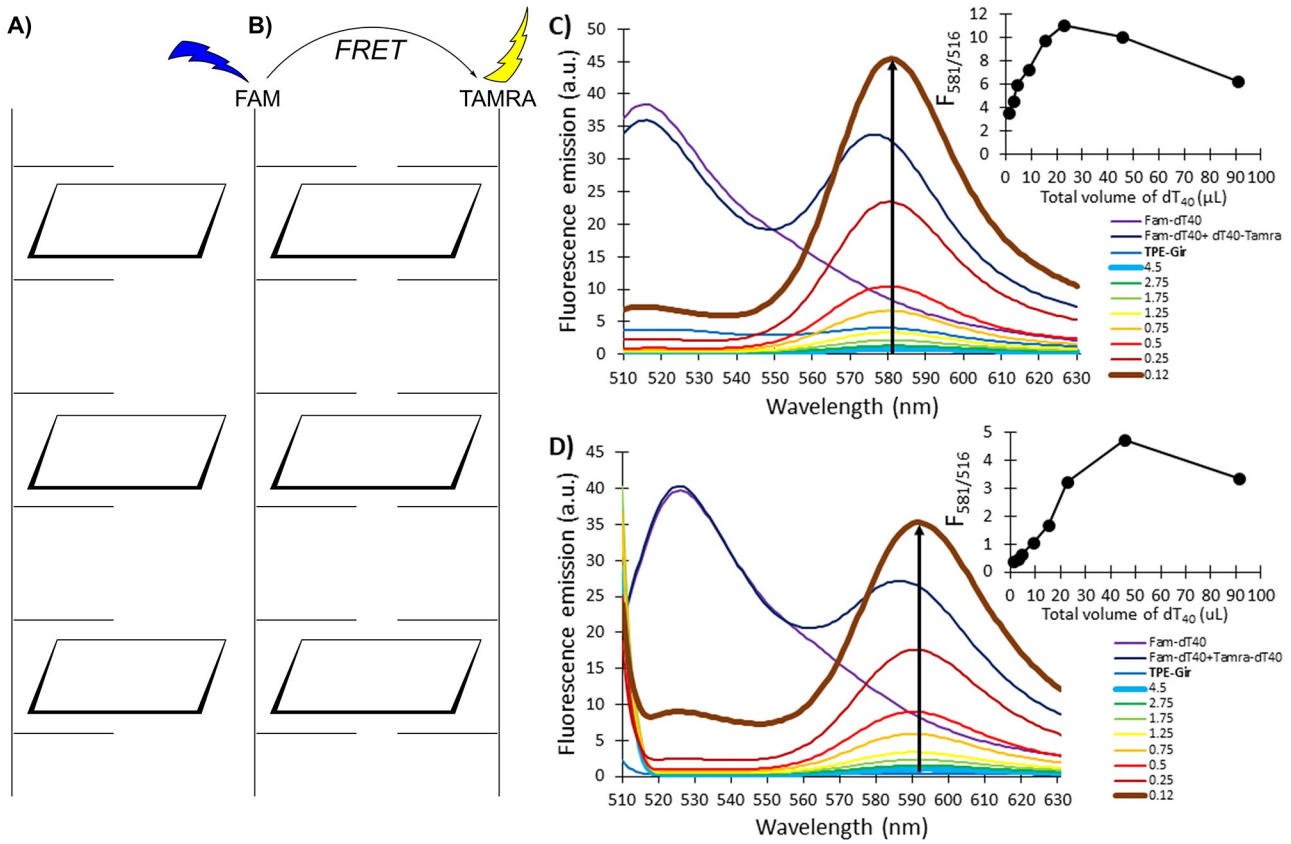

Figure 4. Schematic representation of the different binding modes of a π-conjugated ligand in **A)** single ssDNA following a nearest neighbor site exclusion principle, **B)** two ssDNA strands arranged in parallel/antiparallel pseudo-duplexes which formation can be evidenced using a FRET assay as depicted here (see text for details) and FRET titration experiments of **TPE-Gir** (0.02 mM) at different molar ratios (4.5-0.12) by **C)** FAM-dT_{40} and dT_{40}-(3′-TAMRA), or **D)** FAM-dT_{40} and (5′-TAMRA)-dT_{40}; insets plotting the F_{581}/F_{516} fluorescence ratio at different ligand per nucleobase molar ratios. Ex. 495 nm, Em. 581 nm.

cent-labelled ssDNA probes with FAM (Ex. 495 nm, Em. 516 nm) and TAMRA (Ex. 520 nm, Em. 581 nm) acting as Fluorescence Resonance Energy Transfer (FRET) donor and acceptor dyes, respectively. The results revealed that upon addition of those two ssDNA probes onto a solution of **TPE-Gir** in saline water (150 mM NaCl), an increasing FRET signal, monitored by the F_{581}/F_{516} fluorescence emission ratio, occurred up to the stoichiometry of 1 ligand per 2 nucleobases where its maximal value – 13-fold greater than without **TPE-Gir** – was reached (Figure 4C). Using (5′-FAM)-dT_{40} and (5′-TAMRA)-dT_{40}, a similar result was obtained with the maximum of the F_{581}/F_{516} fluorescence emission ratio reached at the stoichiometry of 1 ligand per 4 nucleobases. However, the magnitude of the FRET signal was limited to a 4-fold increase compared to the experiment conducted in the absence of **TPE-Gir** (Figure 4D). These results confirm the formation of the ligand-templated *pseudo-duplexes* (Figure 4B) and show that an antiparallel arrangement of the two ssDNA strands remains preferred compared to a parallel arrangement. Given the previously-determined binding stoichiometry of 1 ligand per 3 nucleobases, most likely the two proposed binding models – partial "intercalation-like" of **TPE-Gir** in a single ssDNA strand and ligand-templated pseudo-duplex formation – depicted in Figure 4A and Figure 4B respectively, co-exist in a dynamic equilibrium in the conditions used in this study. The F_{581}/F_{516} fluorescence emission ratio strongly and gradually decreases with heating (Figure S3, ESI), confirming a statistical non-cooperative pseudo duplex formation. The process is fully reversible over a complete cooling/heating cycle.

Interaction with double-stranded DNA. Interaction with dsDNA can take place through intercalation, groove-binding, or outside binding – the latter occurring by salt bridge interactions with the phosphodiester backbone and is usually promoted in conditions of low salinity. Spectroscopic analyses were carried out using calf-thymus DNA. The spectroscopic data match those previously obtained with ssDNA in that UV-Vis absorption spectroscopy show hypo- and batho-chromic shifts when adding dsDNA, the fluorescence emission gradually increases at 515 nm, and CD spectroscopy shows a negative ICD signal at 310 nm (Figure 5). Not surprising given the more defined helical arrangement of dsDNA, the molar ellipticity in this case is much higher than with ssDNA (compare Figure 5C with Figure 3C). The Job plot analysis reveals a binding stoichiometry around 1 ligand per 3 base pairs, in fairly good agreement with the nearest neighbor site exclusion principle, which could suggest a binding through intercalation (Figure 5D).[40] However, it is important to be cautious regarding the interpretation of ICD signals, given the different mechanisms that contribute to these

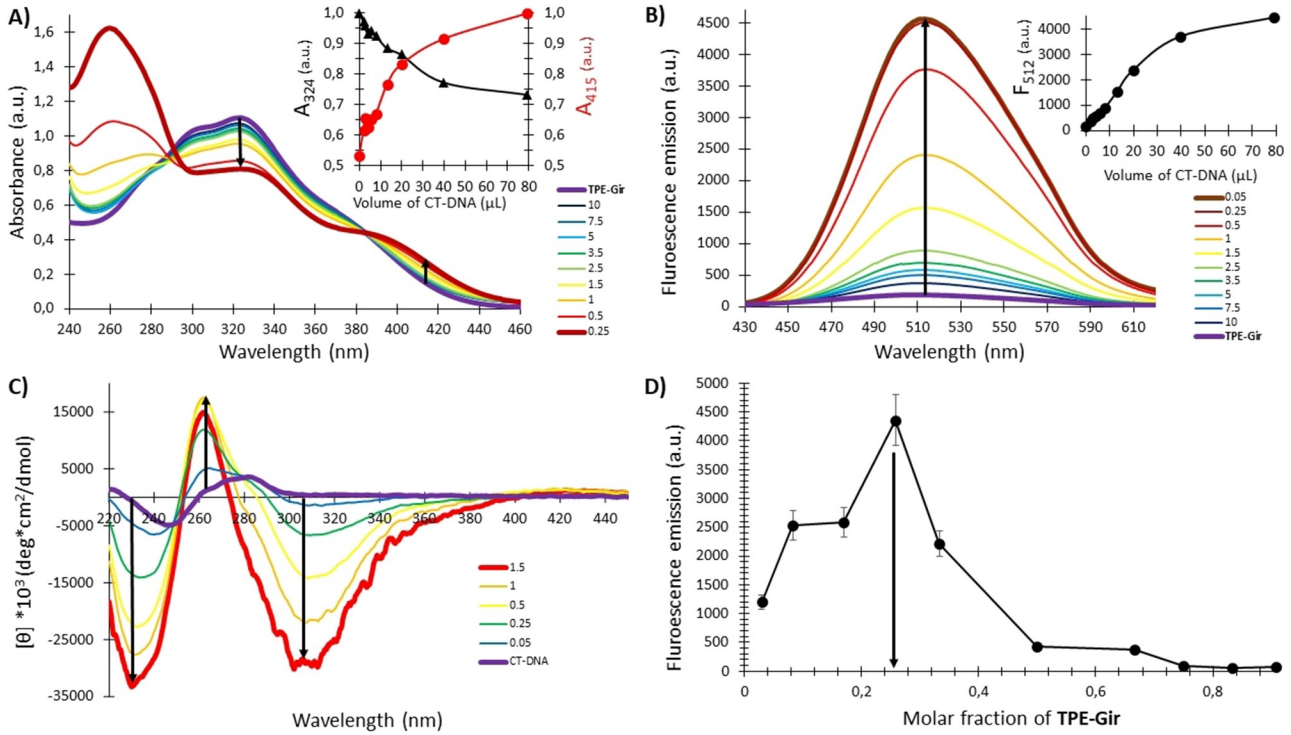

Figure 5. A) UV-Visible titration of **TPE-Gir** (0.02 mM in HEPES) by CT-DNA at different molar ratios (final concentrations of 0.1 nM to 4 nM). **Inset**: Normalized evolution of **TPE-Gir**: CT-DNA absorbances at different volumes of CT-DNA (λ_{exc} = 324 and 415 nm); **(B)** Fluorescence emission spectra of **TPE-Gir** (0.02 mM in HEPES) by CT-DNA at different molar ratios (final concentrations of 0.1 nM to 4 nM) (λ_{exc} = 310 nm). **Inset**: Fluorescent emission evolution of **TPE-Gir**:CT-DNA spectra at different volumes of CT-DNA (λ_{em} = 515 nm); (C) CD titration spectra of CT-DNA (final concentration of 2.11 nM in water) by **TPE-Gir** at different molar ratios in H_2O (final concentration of **TPE-Gir** of 2 µM to 60 µM); (D) Job plot obtained through fluorescence titration experiments (relative error of 10% applied). The molar ratios are expressed in ligand per base pair. HEPES buffer: 10 mM HEPES, 9.4 mM NaCl, 10 µM EDTA, pH 7.2.

signals, as detailed for a dsDNA minor groove binder such as DAPI (4′,6-diamidino-2-phenylindole).[41] Interestingly, we can also notice, from the CD spectra, changes in DNA structure (positive band shifted from 280 to 260 nm; negative band shifted from 245 to 230 nm) that could indicate a B-to-A helix conversion in the presence of **TPE-Gir** (Figure 5C).[42] The marked AIE effect was further evidenced in gel electrophoresis experiments where luminescent bands for complexed plasmids are observed when irradiated at 320 nm (Figure S3, ESI) – an essential but not sufficient prerequisite for "light-up" probes.[25b,26a]

Interaction with DNA G-quadruplexes. G-quadruplexes (G4s) are folded secondary structures of nucleic acids, formed in guanine-rich sequences that are assembled into stacks of planar G-quartets in the presence of templating monovalent cations. DNA G4s are present in telomeres and their abnormal persistence has been linked to cancer cells avoiding entering senescence/apoptosis. Therefore, ligands that would interact and stabilize G4s in tumor cells so that telomere repair by telomerases is inhibited, ultimately restoring senescence/apoptosis, bear a strong pharmaceutical interest.[43] Examples of ligand families are acridines, bisquinoliniums, porphyrin, naphthalene- and perylene-diimides which interact with G4 targets by electrostatic interactions with the loops and by π-type interactions with G-quartets.[44] In this line, we have recently evidenced the selective binding of different ligands for G4s,[45] including some based on TPE that have also been explored by us[26a] and others,[26d] finding important effects related to the nature of the spacers connecting the central aromatic core with the peripheral cationic groups.[26b,c] Due to the strong propensity of **TPE-Gir** to engage in π stacking interactions with nucleobases and its original acylhydrazone spacer, we were interested in its binding properties to G4s. We have selected a human telomeric DNA sequence Tel22 (5′-AGG GTT AGG GTT AGG GTT AGG G-3′) for its biological relevance. This sequence has been shown to adopt an anti-parallel conformation in presence of 100 mM Na^+, while it adopts mixed parallel and antiparallel conformations in presence of K^+.[46] Indeed, CD spectra of Tel22 in Tris-EDTA (TE) buffer in absence and in presence of K^+ show positive and negative peaks, at 293 nm and 235 nm respectively, indicative of hybrid G4s conformations, which may differ in loop arrangement, strand orientations and tetrad arrangements. In the presence of Na^+, the anti-parallel conformation is preferred as indicated by specific CD signals (positive at 295 nm and negative at 262 nm) (Figure 6A).[47] In presence of **TPE-Gir**, for a Tel22:**TPE-Gir** (1:1) mixture, the CD signature of the anti-parallel conformation is globally maintained, although different intensities are noted. In contrast, Tel22 binding by **TPE-Gir** in a 1:5 ratio produces a hybrid topology. The hybrid is characterized by a positive CD signal at 292 nm with a distinct shoulder at ~270 nm as well as a strong negative peak at 235 nm. The G4-ligand interaction is

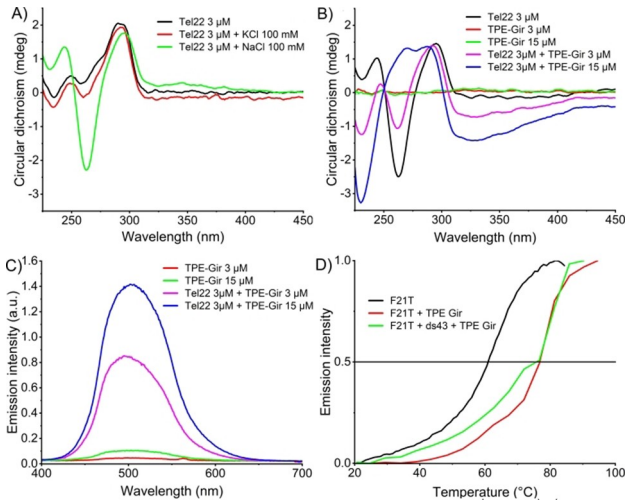

Figure 6. A) CD Spectra of pure Tel22 (3 µM) in TE buffer (pH 7.4), in presence of 100 mM K^+ and 100 mM Na^+ ; B) CD Spectra of pure Tel22 (3 µM), pure **TPE-Gir** (3 µM and 15 µM) and Tel22:**TPE-Gir** mixture at 1:1 and 1:5 molar ratio in TE buffer (pH 7.4) in presence of 100 mM Na^+ ; C) Fluorescence emission spectra (λ_{exc} = 269 nm) of pure **TPE-Gir** (3 and 15 µM) and Tel22:**TPE-Gir** mixture at 1:1 and 1:5 molar ratio in TE buffer in presence of 100 mM Na^+ ; D) Thermal denaturation by FRET assay using F21T alone, F21T:**TPE-Gir** mixture (1:5 molar ratio) and F21T:**TPE-Gir**:ds43-dsDNA mixture (1:5:10 molar ratio) with dsDNA ds43 as competitor in lithium-cacodylate buffer (10 mM, 100 mM K^+, pH 7.2). The FAM emission at 516 nm (λ_{exc} = 492 nm) has been normalized.

also evidenced by the broad negative ICD signal observed in the 310–350 nm range where **TPE-Gir** absorbs, due to the induction of chirality from G4 to **TPE-Gir** (Figure 6B). Fluorescence emission spectra show a strong enhancement (~ 15 fold) and a small (10 nm) red-shift of the emission band of **TPE-Gir** in the presence of G-quadruplex (Figure 6C). Finally, we assessed the stabilization of G-quadruplex and the binding selectivity of **TPE-Gir** by thermal denaturation through a FRET assay.[48] For this purpose, we used a modified Tel22, named F21T, appended with a FAM dye at position 5′ and a TAMRA dye at position 3′.[26a] The results show a significant increase in the melting temperature ($\Delta T_{1/2}$ = 16 °C) that indicates a strong stabilization of this G4 structure (Figure 6D). This value is close to that reported for tetraimidazolium tetraphenylethene (TPE–Im) ($\Delta T_{1/2}$ = 19.5 °C)[26a] and slightly lower than ligands with larger aromatic cores such as tetrakis(N-methylpyridinium-4-yl)porphyrin ($\Delta T_{1/2}$ = 23 °C) or tetraimidazolium-fused porphyrin ($\Delta T_{1/2}$ = 25 °C).[45c] Nevertheless, no decrease of this melting temperature is noted after addition of 10 equivalents of a random sequence dsDNA (with 43 base pairs), which points toward a great selectivity of **TPE-Gir** for G4 compared to dsDNA, possibly due to more important π-π interactions (see below).

Determination of binding constants. Isothermal titration calorimetry (ITC) experiments were carried out in order to estimate the equilibrium association constants (K_a) between **TPE-Gir** and nucleic acids, in particular with two very different types of nucleic acids (ssDNA dT_{40} and G-quadruplex Tel22). Table 1 provides the thermodynamic parameters in two buffered solutions containing either 150 mM NaCl or KCl.

Table 1. Thermodynamic parameters derived from Isothermal Titration Calorimetry binding studies for the binding of **TPE-Gir** to ssDNA dT_{40} and G-quadruplex Tel22. Experiments were conducted in a TE buffer (50 mM, pH 6.5), in presence of 150 mM NaCl (Na^+ form) or 150 mM KCl (K^+ form).

	dT_{40}, Na^+ buffer	dT_{40}, K^+ buffer	Tel22, Na^+ form	Tel22, K^+ form	
K_d (µM)	17	14	3.8	0.7	7
K_a (10^6 M^{-1})	0.06 ±0.01	0.07 ±0.01	0.26 ±0.1	1.53 ±0.3	0.14 ±0.02
ΔH (kcal.mol^{-1})	-6.24 ±0.1	-6.9 ±0.1	-2.9 ±0.3	0.10 ±0.1	2.47 ±0.1
-TΔS (kcal.mol^{-1})	−0.15	0.45	−4.4	n.d.	−9.4
Stoechiometry [ligand/DNA]	11–14	11–14	0.5	0.5–1	4

The interactions with dT_{40} is salt-independent and appears enthalpy-driven with a moderate association constant K_a = 6.5 10^4 M^{-1} (Table 1). This value, along with the binding stoichiometry of around 11–14 ligands per dT_{40} (i.e. 1 ligand per 2.8–3.6 nucleobase) fits very well the data previously obtained by the Job plot method (1 ligand per 3 nucleobases, *vide supra*). From these data, one can calculate[6b] that 96% of **TPE-Gir** ligands are bound under these conditions.

The thermodynamic parameters for **TPE-Gir** with Tel22 are markedly different. First, an obvious salt effect was observed (Table 1). While a single exothermic binding profile was observed for the interaction of **TPE-Gir** with Tel22 in its Na^+ form – with an affinity of 2.6×10^5 M^{-1} and a stoechiometry of 0.5, the shape of the ITC isotherm for **TPE-Gir** binding to Tel22 in its K^+ form indicated a biphasic binding event. In this two-site binding profile, an initial binding event ($K_a = 1.4\times10^5$ M^{-1}) requiring a low **TPE-Gir**/Tel22 ratio to reach saturation was first observed, followed by a stronger secondary process ($K_a = 1.53\times10^6$ M^{-1}). A possible explanation for such two-step binding could be that the initial binding of **TPE-Gir** induces a conformational rearrangement of Tel22, forcing the G-quadruplex to adopt a unique fold (1st binding event – stoichiometry in the same range than in Na^+ conditions), while additional ligands are subsequently externally bound (2nd binding event, N = 4) as previously shown.[49] Overall, these data confirm that **TPE-Gir** polyintercalate weakly in ssDNA and displays selective binding to G quadruplexes with sensitivity to the structure ($K_{a,\ Tel22}/K_{a,\ dT40}$ = 4.33, $\Delta(\Delta G°)$ = 0.9 kcal.mol^{-1}). In contradiction to our previous results,[50] binding to CT-DNA could unfortunately not be properly quantified by ITC in those conditions. Instead, the corresponding binding constant was determined from the UV-Vis titration (Figure 5A), monitored at 325 and 430 nm, using the Benesi-Hildebrand equation.[51] An apparent binding constant $K_a = 3.7–10.8\times10^4$ M^{-1} was determined, which confirms a weaker binding of **TPE-Gir** to CT-DNA as compared to G-quadruplex Tel22.

Docking simulations: Interactions with G4 (human telomeric sequence Tel22). Docking studies were performed to decipher the binding modes of **TPE-Gir** with Tel22 (in Na^+ conditions, PDB ID: 143D), taking into account indirectly the flexibility of G4 through calculations on several conformations

available from NMR coordinates, see methodology in the Supplementary Information). The most stable docking solution depicts a **TPE-Gir** binding mode in a wide groove of Tel22 (see Figure 7). Given the branched and propeller-like conformation of **TPE-Gir**, numerous close contacts, were observed with several residues along the G4 target (i.e. 86 contacts at a distance < 3.5 Å), in particular π-type interactions between **TPE-Gir** aromatic core and four guanine residues (G2/G10 from the first tetrad and G3/G9 from second tetrad, see Figure 7A), some in a perpendicular (T-shape) interaction mode. In addition, a series of H-bonds and electrostatic interactions between the quaternary ammoniums at the **TPE-Gir** extremities with Tel22 were observed, (see details in Figure 7 B–D). Regarding the **TPE-Gir** 'wings' labelled #1, #2 and #3 in Figure 7A, five H-bonds involving **TPE-Gir** amide fragments were found. Moreover, two cationic quaternary ammoniums of **TPE-Gir** (wings #2 and #3) are close to phosphate groups of Tel22 (5.8 and 6.3 Å for N–P distances, see Figure 7C–D), a distance that can likely evolve regarding the flexibility of terminal groups in the four wings of **TPE-Gir**. Only one branch of **TPE-Gir** (wing #4) points outside the core of the target, without any particular close contact. Globally, the binding mode of **TPE-Gir** ligand within a G4 groove therefore involves a series of electrostatic interactions, H-bonds and π-type interactions, distributed differently among the four wings of **TPE-Gir**.

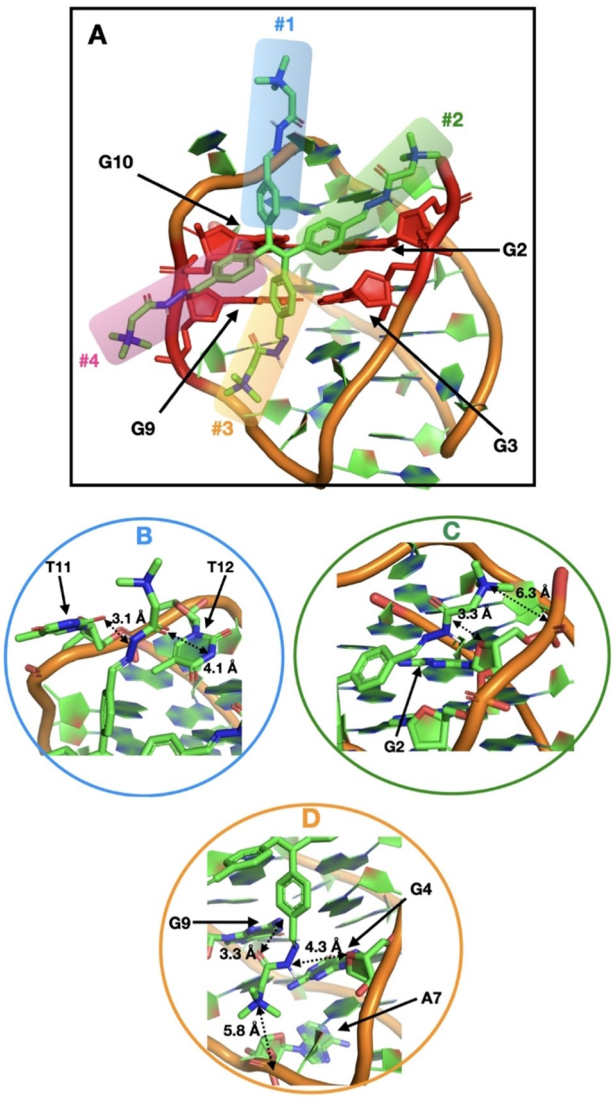

Figure 7. A. Most stable docking solution of **TPE-Gir** (stick representation, green) in the groove of Tel22 (cartoon representation, conformation #1 from PDB ID: 143d). The four wings of **TPE-Gir** are labelled from #1 to #4. The four guanine residues that are involved in stacking interactions with **TPE-Gir**, i.e., G2/G10 (1st tetrad) and G3/G9 (2nd tetrad), are represented in sticks (color red); B–D. Zooms on the interactions between **TPE-Gir** wing and Tel22 (see colour code for the wing number in A).: H-bonds and electrostatic interactions are highlighted with black arrows.

Docking simulations: Interactions with DNA. For docking calculations with a dsDNA, a double helix of 43 base pairs was considered. Our docking protocol was repeated with different docking parameters to increase the probability of finding the minimum binding energy of the **TPE-Gir**/dsDNA complex (see computational details, Figures S8–S9). The most stable binding mode shows a binding of **TPE-Gir** in a DNA minor groove (Figure 8). Two wings of the ligand (#2 and #3, see Figure 8), are deeply docked in the minor groove whereas the two other wings point in opposite directions. The two deeply docked aromatic moieties are not involved in π-type interactions (as was observed for **TPE-Gir**/G4 complex) but rather in van der Waals interactions with dsDNA backbone. The four quaternary ammonium groups of **TPE-Gir** are all involved in electrostatic interactions with DNA phosphate groups (Figure 8B–D), in contrast to what was observed for **TPE-Gir**/Tel22 complex, in which only 2 wings over 4 were involved in electrostatic interactions. In comparison with **TPE-Gir**/Tel22 complex, the affinity of the **TPE-Gir** ligand to dsDNA is thus coming from numerous and stronger electrostatic interactions (but no π-type interactions). Although the propeller conformation of TPE core is unlikely to enter in between dsDNA base pairs, it is worth mentioning that our docking simulations in a rigid target approach limits the possibilities to find intercalation modes. Therefore, intercalation in between base pairs, although unlikely from our experience, cannot be totally excluded. The minor groove binding could be a first step with a subsequent intercalation process, facilitated by the electrostatic anchoring of the four **TPE-Gir** wings along dsDNA.

Conclusion

We reported herein the design, synthesis, self-assembly and nucleic acid recognition of a novel ligand featuring a tetraphenylethene aromatic core tethered to four quaternary ammonium groups through acylhydrazone spacers. We found that this compound leads to the formation, in water/THF mixtures, of fluorescent nanoparticles having diameters around 100–120 nm. Detailed spectroscopic studies using single- and double-stranded DNA as templates reveal the strong propensity to intercalate into single-stranded DNA, the ability to bind into the minor groove of double-stranded DNA, and the selective binding to G-quadruplex. Finally, a selective binding of DNA G-quadruplex was evidenced. Those recognition events are

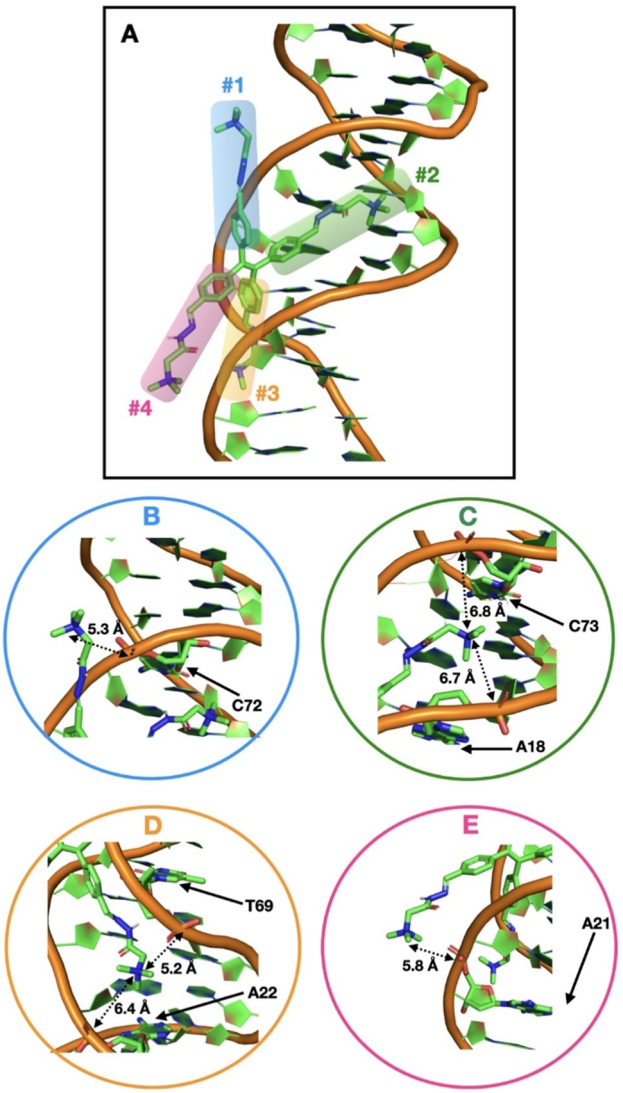

Figure 8. A. Zoom on the most stable docking solution of **TPE-Gir** (stick representation, green) in the minor groove of a model DNA (cartoon representation). The four wings of **TPE-Gir** are labelled from #1 to #4; B–D. Zooms on the electrostatic interactions between **TPE-Gir** wings and dsDNA (see colour code for the wing number in A). Distances were measured between N and P atoms.

quantified by isothermal titration calorimetry and the proposed binding models are supported by docking simulations. Given the versatility of the acylhydrazone ligation technique[28a] as well as the ability of this group to undergo photo-switching,[52] there is plenty of room to expand the approach described here and tether different end-groups for fine-tuning self-assembly properties and modulate nucleic acids recognition.

Experimental Section

General procedures and materials. All solvents and reagents were purchased from commercial suppliers and used without further purifications. Oligonucleotides were purchased from Eurogentec as RP-Cartridge purification (dT_{40}) or RP-HPLC purification for FAM-dT_{40}, TAMRA-dT_{40}, and dT_{40}-TAMRA (Ultrapure Gold, >95% purity) in dried format or from Sigma Aldrich for CT-ssDNA and CT-DNA. **TPE-Ald** was synthesized according to reported literature procedure.[27]

NMR. ^{1}H Nuclear Magnetic Resonance (NMR) spectra were recorded at 400 MHz (Bruker Avance 400) using deuterated water. Chemical shifts are reported in ppm relative to the residual solvent peak. Data are reported as follows: Chemical shifts (δ), multiplicity (s for singlet, d for doublet, and m for multiplet), integration and coupling constant (^nJ in Hertz).

Mass spectrometry. Mass spectrometry analyses (positive mode) were carried out in the Laboratoire de Mesures Physiques, Université de Montpellier using a Micromass Q-Tof instrument.

HPLC. HPLC analyses were performed on a Waters HPLC 2695 (EC Nucleosil 300–5 C_{18}, 125×3 mm) column, Macherey – Nagel) equipped with a Waters 996 DAD detector. The following linear gradients of solvent B (90% acetonitrile, 9.9% water, and 0.1% TFA) into solvent A (99.9% water and 0.1% TFA) were used: 0 to 95% of solvent B in 5 min; flow 1 ml/min. Retention time (t_R) are given in minutes. Semi-preparative RP-HPLC were performed on a Waters 515 HPLC (VP Nucleodur 250–21 C18, HTec 7 μm column, Macherey-Nagel) equipped with a Waters 2487 detector.

UV-Vis absorption and CD spectroscopy. UV-Vis absorption spectra were recorded at 20°C on a UV-31 OOPC UVisco spectrophotometer in 10 mm quartz cells (Hellma). The spectra were recorded at 20°C between 200 and 650 nm, with a bandwidth of 1 nm, time per point 1 s. For studies with ssDNA and dsDNA, CD spectra were recorded at 20°C using 10 mm and 2 mm quartz cells (Hellma) at the Laboratoire de Mesures Physiques, IBMM – Université de Montpellier. For studies with G-quadruplexes, UV-Vis absorption measurements were recorded using a ChirascanTM Plus CD Spectrometer (Applied Photophysics) at the University of Mons. The measurements were carried out using 2 mm suprasil quartz cells from Hellma Analytics. The spectra were recorded at 20 °C between 225 nm and 600 nm, with a bandwidth of 1 nm, time per point 1 s. The buffer water solvent was Tris-EDTA (TE) prepared from 1 M Tris-Cl and 0.5 M EDTA to achieve a 10 mM Tris-Cl and 1 mM EDTA final buffer at pH 7.5. The buffered water solvent reference spectra were used as baselines and were automatically subtracted from the CD and UV-vis absorption spectra of the samples. All the spectra were plotted by using OriginPro 2018 software.

Fluorescence spectroscopy. Fluorescence analyses were carried out on a HITACHI fluorescence spectrophotometer F-2500. For studies with G-quadruplexes, emission spectra of **TPE-Gir**/oligonucleotides mixtures were recorded at the University of Mons using a ChirascanTM Plus CD spectrophotometer (Applied Photophysics) equipped for fluorescence measurements. The measurements were carried out using 4 mm by 10 mm suprasil quartz cells from Hellma Analytics. The spectra were recorded at 20 °C between 350 and 650 nm with an excitation wavelength at 269 nm and a bandwidth of 1 nm.

Dynamic Light Scattering. Particle size measurements were carried out at 25 °C from a 0.025 mM solution of **TPE-Gir** in 3 mL THF/H_2O 99/1 (v/v) on a Zetasizer Nano ZS (Malvern, United Kingdom) using 10 mm quartz cells (Hellma).

Fluorescence Resonance Energy Transfer (FRET) Assays. FRET assays were performed using FAM-dT_{40}, TAMRA-dT_{40} and dT_{40}-TAMRA. The fluorescence emission spectra were recorded at 20 °C on a fluorescence spectrophotometer FLX-Xenius XMF using λ_{ex} = 495 nm and λ_{em} = 500-650 nm.

Isothermal Titration Calorimetry. The thermodynamic binding parameters were recorded at 20 °C on a MicroCal/Malvern PEAK-ITC

(Malvern Panalytics) instrument. The titration cell was filled with a solution of 25 μM single-stranded dT_{40} DNA or Tel22, and the syringe was loaded with a 0.3–3 mM solution of **TPE-Gir**. For each experiment, a series of injections of ligand from a rotating syringe (speed 750 rpm) were made into the thermostatic cell (initial delay of 60 s, duration of 2 s and spacing of 120 s). Control experiments were performed by adding the ligand solution to the cell containing the buffer. The corrected ITC titrations were processed using the MicroCal Origin software.

Transmission Electronic Microscopy. Transmission Electron Microscopy (TEM) was carried out at the plateforme de Microscopie Électronique et Analytique, Université de Montpellier using a JEOL 1200 EXII 120 kV instrument.

Molecular Docking. TPE-Gir was built within the Avogadro molecular editor.[53] Molecular mechanics calculations were then performed to optimize the geometry of the **TPE-Gir** molecule. For this, a two-step minimization procedure, i.e., a steepest descent optimization followed by a conjugate gradient optimization (10,000 steps), was performed with the General Amber Force Field (GAFF).[54] The energy convergence criterion was set at 10^{-7} kJ.mol^{-1} for the energy minimization. The coordinates of the G-quadruplex (G4) were obtained from the Protein Data Bank (PDB ID: 143D). The NMR conformations of the G4 were extracted to perform ensemble docking calculations, i.e., six conformations for the 143D target. Docking calculations were performed with the *QuickVina-W* package,[55] a fork of AutoDock Vina package, optimized for wide search space and blind docking.[56] As we have no *a priori* knowledge of the **TPE-Gir** binding mode along the G4 structure, a sufficiently large grid was built around each G4 conformation to allow the exploration of the entire G4 surface during the docking calculations. A large grid size of 40×40×40 Å^3 with a spacing of 1.0 Å was thus considered. The center of the grid box was located on the centre-of-mass of the G4 targets. Our docking protocol was repeated with several docking algorithm parameters to increase the probability of finding the minimum binding energy of the complex. As the grid presents an important size, a starting exhaustiveness value of 64 was chosen, a larger one than the default value, i.e., eight.[57] The docking simulations were then replicated with larger exhaustiveness values, i.e., 128, 256, 512 and 1024, to ensure the convergence of the optimum docking solution. **TPE-Gir** was set as a flexible entity with flexibility on torsions of the terminal groups of the four **TPE-Gir** wings. The 10 most energetically favourable complexes were retained for each docking calculation. The PyMOL molecular visualization system was used to depict the results docking calculations.[58] For the calculations on **TPE-Gir**/Tel complex, for each replica of our docking protocol, the best docking solution was always obtained with the conformation #1 of Tel22 (see docking scores in Figure S6). Moreover, a very similar **TPE-Gir** binding mode is observed from the superimposition of the best docking solutions issued from each docking replica, which indicates a reliable convergence of the docking search algorithm (Figure S7). For the **TPE-Gir**/dsDNA complex, the replica converge to a very similar docking solution regarding both the binding energy scores (Figure S8) as well as on the geometries, see the superimposition of the best docking poses for each replica in Figure S9.

Synthesis and characterization of TPE-Gir. TPE-Ald (11.3 mg, 25.4 μmoles) and Girard's reagent T (38.2 mg, 226.5 μmoles, 8 eq.) were mixed in ethanol (2 mL) and the reaction mixture was stirred at reflux overnight. The desired product was isolated in 71% yield by semi-preparative reverse-phase HPLC (linear gradient $H_2O \rightarrow H_2O$/acetonitrile 80/20 in 20 mins). ^{1}H NMR[59] (D_2O) shows a 7/3 mixture of 2 isomers, most probably E/Z acylhydrazone isomers: 8.16 (s, 0.7 H, H_c), 7.94 (s, 0.3 H, $H_{c'}$), 7.56 (d, $^3J_{H\text{-}H}$ = 8.0, 1.3 H, H_a/H_b), 7.52 (d, $^3J_{H\text{-}H}$ = 8.4, 0.7 H, $H_{a'}/H_{b'}$), 7.23 (m, 2H, $H_a/H_b + H_{a'}/H_{b'}$), 4.68 (s, 0.6 H, $H_{d'}$), 4.20 (s, 1.3 H, H_d), 3.34 (s, 9H, H_e); ESI-MS: calcd for $[C_{50}H_{68}N_{12}O_4]^{4+}$ 225.1366, found 225.1379; $[C_{50}H_{68}N_{12}O_4\text{-}H]^{3+}$ 299.8464, found 300.18; $[C_{50}H_{68}N_{12}O_4\text{-}2H]^{2+}$ 449.2660, found 449.27.

Preparation of ligand in water/THF mixtures for AIE studies. The Aggregation-Induced Emission (AIE) effect was determined by preparing solution of 6 μL **TPE-Gir** (10 mM in water) in 3 mL (final concentration 0.02 mM) in different solvent ratio of THF in H_2O (0%, 20%, 50%, 70%, 90%, 95%, 96%, 97%, 98%, 99%).

Preparation of ligand:oligonucleotide complexes. UV-Vis and fluorescence titration experiments using ssCT-DNA, dT_{40}, CT-DNA (stock solutions in water, 0.16 μM for ssCT-DNA and CT-DNA and 133 μM for dT_{40}), were carried out in 10 mm quartz cells by mixing 6 μL of a 10 mM solution of **TPE-Gir** (final concentration of **TPE-Gir** 0.02 mM) and oligonucleotides (final concentrations of 0.2 nM to 8 nM for ssCT-DNA and 0.1 nM to 4 nM for CT-DNA) in HEPES. Similarly, CD spectroscopy analyses were carried out by mixing 19.6 μL of a solution of dT_{40} (final volume of 200 μL) and **TPE-Gir** (final concentrations of 0.012 mM to 0.6 mM) in 2 mm quartz cells, or 39.6 μL of a solution of CT-DNA (final volume of 3 mL) and **TPE-Gir** (final concentrations of 2 μM to 60 μM) in 10 mm quartz cells. Molar ratios vary between 0.5 and 10 and are expressed in ligand per nucleobase for ssDNA/dT_{40}, and ligand per base pair for dsDNA.

Acknowledgements

We thank the ANR (ANR-17-CE07-0042-01) for funding. Research in Mons was supported by the University of Mons, the Wallonia Region, and the Fund for Scientific Research (F.R.S.-FNRS) under the grant EOS No. 30650939 (PRECISION). SR and CK acknowledge the Région Languedoc-Roussillon (Research Grant "Chercheur(se)s d'Avenir-2015-005984) and the FEDER program (Fonds Européen de Développement Régional) for funding. CK also thanks UMONS for a Ph.D. grant. We thank Dr. Prisca Boisguerin and Dr. Sébastien Deshayes for access to the DLS instrument, Emeric Audfray for assistance with the MicroCal PEAK-ITC equipment (Malvern Panalytical), Dr. Erwan Oliviero for assistance with the TEM analyses, and Dr. Baptiste Legrand for assistance with CD. Computational resources have been provided by the Consortium des Équipements de Calcul Intensif (CÉCI), funded by the F.R.S.-FNRS under Grant No. 2.5020.11 and by the Wallonia Region.

Conflict of Interest

The authors declare no conflict of interest.

Keywords: Aggregation induced emission · G-quadruplex · Molecular recognition · Nucleic acids · Self-assembly

[1] S. Cantekin, T. F. A. de Greef, A. R. A. Palmans, *Chem. Soc. Rev.* **2012**, *41*, 6125–6137.
[2] a) M. F. J. Mabesoone, S. Kardas, H. Soria-Carrera, J. Barberá, J. M. de la Fuente, A. R. A. Palmans, M. Fossépré, M. Surin, R. Martin-Rapún, *Mol Syst Des Eng* **2020**, *5*, 820–828; b) C. Kulkarni, E. W. Meijer, A. R. A. Palmans, *Acc. Chem. Res.* **2017**, *50*, 1928–1936.
[3] Y. Yang, M. W. Urban, *Chem. Soc. Rev.* **2013**, *42*, 7446–7467.
[4] a) S. van Dun, J. Schill, L. G. Milroy, L. Brunsveld, *Chem. Eur. J.* **2018**, *24*, 16445–16451; b) M. H. Bakker, C. C. Lee, E. W. Meijer, P. Y. W. Dankers, L. Albertazzi, *ACS Nano* **2016**, *10*, 1845–1852; c) K. Petkau-Milroy, L. Brunsveld, *Org. Biomol. Chem.* **2013**, *11*, 219–232; d) K. Petkau-Milroy,

M. H. Sonntag, L. Brunsveld, *Chem. Eur. J.* **2013**, *19*, 10786–10793; e) D. A. Uhlenheuer, K. Petkau, L. Brunsveld, *Chem. Soc. Rev.* **2010**, *39*, 2817–2826.
[5] M. Surin, S. Ulrich, *ChemistryOpen* **2020**, *9*, 480–498.
[6] a) J. Rubio-Magnieto, T. A. Phan, M. Fosséprè, V. Matot, J. Knoops, T. Jarrosson, P. Dumy, F. Serein-Spirau, C. Niebel, S. Ulrich, M. Surin, *Chem. Eur. J.* **2018**, *24*, 706–714; b) S. M. Hafshejani, S. M. D. Watson, E. M. Tuite, A. R. Pike, *Chem. Eur. J.* **2015**, *21*, 12611–12615; c) S. Moradpour-Hafshejani, J. H. Hedley, A. O. Haigh, A. R. Pike, E. M. Tuite, *RSC Adv.* **2013**, *3*, 18164–18172; d) K. C. Hannah, B. A. Armitage, *Acc. Chem. Res.* **2004**, *37*, 845–853; e) M. M. Wang, G. L. Silva, B. A. Armitage, *J. Am. Chem. Soc.* **2000**, *122*, 9977–9986.
[7] L. Albertazzi, F. J. Martinez-Veracoechea, C. M. A. Leenders, I. K. Voets, D. Frenkel, E. W. Meijer, *Proc. Natl. Acad. Sci. USA* **2013**, *110*, 12203–12208.
[8] P. Evenou, J. Rossignol, G. Pembouong, A. Gothland, D. Colesnic, R. Barbeyron, S. Rudiuk, A. G. Marcelin, M. Menand, D. Baigl, V. Calvez, L. Bouteiller, M. Sollogoub, *Angew. Chem. Int. Ed.* **2018**, *57*, 7753–7758; *Angew. Chem.* **2018**, *130*, 7879–7884.
[9] Y. Zhang, E. Petit, M. Barboiu, *ChemPlusChem* **2018**, *83*, 354–360.
[10] P. G. A. Janssen, S. Jabbari-Farouji, M. Surin, X. Vila, J. C. Gielen, T. F. de Greef, M. R. Vos, P. H. Bomans, N. A. Sommerdijk, P. C. Christianen, P. Leclère, R. Lazzaroni, P. van der Schoot, E. W. Meijer, A. P. H. J. Schenning, *J. Am. Chem. Soc.* **2009**, *131*, 1222–1231.
[11] a) D. Paolantoni, S. Cantel, P. Dumy, S. Ulrich, *Int. J. Mol. Sci.* **2015**, *16*, 3609–3625; b) D. Paolantoni, J. Rubio-Magnieto, S. Cantel, J. Martinez, P. Dumy, M. Surin, S. Ulrich, *Chem. Commun.* **2014**, *50*, 14257–14260.
[12] a) N. Laroui, M. Coste, L. Lichon, Y. Bessin, M. Gary-Bobo, G. Pratviel, C. Bonduelle, N. Bettache, S. Ulrich, *Int. J. Pharm.* **2019**, *569*; b) M. V. Ishutkina, A. R. Berry, R. Hussain, O. G. Khelevina, G. Siligardi, E. Stulz, *Eur. J. Org. Chem.* **2018**, *2018*, 5054–5059; c) G. Sargsyan, A. A. Schatz, J. Kubelka, M. Balaz, *Chem. Commun.* **2013**, *49*, 1020–1022; d) L. A. Fendt, I. Bouamaied, S. Thöni, N. Amiot, E. Stulz, *J. Am. Chem. Soc.* **2007**, *129*, 15319–15329.
[13] A. D'Urso, S. Nardis, G. Pomarico, M. E. Fragala, R. Paolesse, R. Purrello, *J. Am. Chem. Soc.* **2013**, *135*, 8632–8638.
[14] J. Rubio-Magnieto, M. Kumar, P. Brocorens, J. Idé, S. J. George, R. Lazzaroni, M. Surin, *Chem. Commun.* **2016**, *52*, 13873–13876.
[15] I. Kocsis, A. Rotaru, Y. M. Legrand, I. Grosu, M. Barboiu, *Chem. Commun.* **2016**, *52*, 386–389.
[16] M. Surin, P. G. A. Janssen, R. Lazzaroni, P. Leclère, E. W. Meijer, A. P. H. J. Schenning, *Adv. Mater.* **2009**, *21*, 1126–1130.
[17] a) P. G. A. Janssen, N. J. M. Brankaert, X. Vila, A. P. H. J. Schenning, *Soft Matter* **2010**, *6*, 1494–1502; b) P. G. A. Janssen, S. Jabbari-Farouji, M. Surin, X. Vila, J. C. Gielen, T. F. A. de Greef, M. R. J. Vos, P. H. H. Bomans, N. A. J. M. Sommerdijk, P. C. M. Christianen, P. Leclere, R. Lazzaroni, P. van der Schoot, E. W. Meijer, A. P. H. J. Schenning, *J. Am. Chem. Soc.* **2009**, *131*, 1222–1231.
[18] E. Bartolami, Y. Bessin, N. Bettache, M. Gary-Bobo, M. Garcia, P. Dumy, S. Ulrich, *Org. Biomol. Chem.* **2015**, *13*, 9427–9438.
[19] G. M. ter Huurne, P. Chidchob, A. G. Long, A. Martinez, A. R. A. Palmans, G. Vantomme, *Chem. Eur. J.* **2020**, *26 (44)*, 9964–9970.
[20] C. Bouillon, Y. Bessin, S. Ulrich, unpublished results.
[21] a) B. Jiang, C. W. Zhang, X. L. Shi, H. B. Yang, *Chinese J Polym Sci* **2019**, *37*, 372–382; b) D. D. La, S. V. Bhosale, L. A. Jones, S. V. Bhosale, *ACS Appl. Mater. Interfaces* **2018**, *10*, 12189–12216; c) Z. J. Zhao, J. W. Y. Lam, B. Z. Tang, *J. Mater. Chem.* **2012**, *22*, 23726–23740.
[22] a) J. Mei, N. L. C. Leung, R. T. K. Kwok, J. W. Y. Lam, B. Z. Tang, *Chem. Rev.* **2015**, *115*, 11718–11940; b) R. T. K. Kwok, C. W. T. Leung, J. W. Y. Lam, B. Z. Tang, *Chem. Soc. Rev.* **2015**, *44*, 4228–4238; c) J. Mei, Y. N. Hong, J. W. Y. Lam, A. J. Qin, Y. H. Tang, B. Z. Tang, *Adv. Mater.* **2014**, *26*, 5429–5479; d) Y. N. Hong, J. W. Y. Lam, B. Z. Tang, *Chem. Soc. Rev.* **2011**, *40*, 5361–5388.
[23] B. Li, T. He, X. Shen, D. T. Tang, S. C. Yin, *Polym. Chem.* **2019**, *10*, 796–818.
[24] L. Xu, Z. C. Zhu, X. Zhou, J. G. Qin, C. L. Yang, *Chem. Commun.* **2014**, *50*, 6494–6497.
[25] a) L. Xu, Z. C. Zhu, D. Q. Wei, X. Zhou, J. G. Qin, C. L. Yang, *ACS Appl. Mater. Interfaces* **2014**, *6*, 18344–18351; b) Y. N. Hong, S. J. Chen, C. W. T. Leung, J. W. Y. Lam, B. Z. Tang, *Chem. Asian J.* **2013**, *8*, 1806–1812.
[26] a) C. Kotras, M. Fosséprè, M. Roger, V. Gervais, S. Richeter, P. Gerbier, S. Ulrich, M. Surin, S. Clément, *Front. Chem.* **2019**, *7*, Article 493; b) Q. Zhang, Y. C. Liu, D. M. Kong, D. S. Guo, *Chem. Eur. J.* **2015**, *21*, 13253–13260; c) Y. N. Hong, H. Xiong, J. W. Y. Lam, M. Haussler, J. Z. Liu, Y. Yu, Y. C. Zhong, H. H. Y. Sung, I. D. Williams, K. S. Wong, B. Z. Tang, *Chem. Eur. J.* **2010**, *16*, 1232–1245; d) Y. N. Hong, M. Haussler, J. W. Y. Lam, Z. Li, K. K. Sin, Y. Q. Dong, H. Tong, J. Z. Liu, A. J. Qin, R. Renneberg, B. Z. Tang, *Chem. Eur. J.* **2008**, *14*, 6428–6437.
[27] W. Drozdz, C. Bouillon, C. Kotras, S. Richeter, M. Barboiu, S. Clement, A. R. Stefankiewicz, S. Ulrich, *Chem. Eur. J.* **2017**, *23*, 18010–18018.
[28] a) D. K. Kölmel, E. T. Kool, *Chem. Rev.* **2017**, *117*, 10358–10376; b) W. G. Skene, J.-M. P. Lehn, *Proc. Natl. Acad. Sci. USA* **2004**, *101*, 8270–8275.
[29] a) N. Zhao, M. Li, Y. L. Yan, J. W. Y. Lam, Y. L. Zhang, Y. S. Zhao, K. S. Wong, B. Z. Tang, *J. Mater. Chem. C* **2013**, *1*, 4640–4646; b) X. L. Yang, N. X. Wang, L. M. Zhang, L. R. Dai, H. W. Shao, X. Y. Jiang, *Nanoscale* **2017**, *9*, 4770–4776.
[30] a) Q. Wang, Q. Zhang, Q. W. Zhang, X. Li, C. X. Zhao, T. Y. Xu, D. H. Qu, H. Tian, *Nat. Commun.* **2020**, *11*; b) A. R. Sapala, S. Dhawan, V. Haridas, *RSC Adv.* **2017**, *7*, 26608–26624.
[31] P. Besenius, G. Portale, P. H. H. Bomans, H. M. Janssen, A. R. A. Palmans, E. W. Meijer, *Proc. Natl. Acad. Sci. USA* **2010**, *107*, 17888–17893.
[32] a) M. Balaz, S. Tannir, K. Varga, *Coord. Chem. Rev.* **2017**, *349*, 66–83; b) M. Surin, *Polym. Chem.* **2016**, *7*, 4137–4150; c) A. Ruiz-Carretero, P. G. A. Janssen, A. Kaeser, A. P. H. J. Schenning, *Chem. Commun.* **2011**, *47*, 4340–4347.
[33] a) H. Chen, S. P. Meisburger, S. A. Pabit, J. L. Sutton, W. W. Webb, L. Pollack, *Proc. Natl. Acad. Sci. USA* **2012**, *109*, 799–804; b) M. C. Murphy, I. Rasnik, W. Cheng, T. M. Lohman, T. J. Ha, *Biophys. J.* **2004**, *86*, 2530–2537; c) B. Tinland, A. Pluen, J. Sturm, G. Weill, *Macromolecules* **1997**, *30*, 5763–5765.
[34] S. Ulrich, P. Dumy, *Chem. Commun.* **2014**, *50*, 5810–5825.
[35] In the present case, the shift to longer wavelength in the absorption spectra is indicative of a better conjugation in the ligand, which is probably due to a better planarization enforced by its stacking with nucleobases.
[36] a) N. C. Garbett, P. A. Ragazzon, J. B. Chaires, *Nat. Protoc.* **2007**, *2*, 3166–3172; b) M. Eriksson, B. Norden, *Method Enzymol* **2001**, *340*, 68–98; c) M. Monnot, O. Mauffret, E. Lescot, S. Fermandjian, *Eur. J. Biochem.* **1992**, *204*, 1035–1039; d) H. Porumb, *Prog. Biophys. Mol. Biol.* **1978**, *34*, 175–195.
[37] N. J. Pritchar, A. Blake, A. R. Peacocke, *Nature* **1966**, *212*, 1360–1361.
[38] H. S. Rye, A. N. Glazer, *Nucleic Acids Res.* **1995**, *23*, 1215–1222.
[39] N. Sinha, L. Stegemann, T. T. Y. Tan, N. L. Doltsinis, C. A. Strassert, F. E. Hahn, *Angew. Chem. Int. Ed.* **2017**, *56*, 2785–2789; *Angew. Chem.* **2017**, *129*, 2829–2833.
[40] a) H. M. Berman, P. R. Young, *Annu. Rev. Biophys. Bioeng.* **1981**, *10*, 87–114; b) R. W. Armstrong, U. P. Strauss, T. Kurucsev, *J. Am. Chem. Soc.* **1970**, *92*, 3174–3181.
[41] N. H. List, J. Knoops, J. Rubio-Magnieto, J. Idé, D. Beljonne, P. Norman, M. Surin, M. Linares, *J. Am. Chem. Soc.* **2017**, *139*, 14947–14953.
[42] J. Kypr, I. Kejnovska, K. Bednarova, M. Vorlıckova, in *Applications in Stereochemical Analysis of Synthetic Compounds, Natural Products, Biomolecules, Vol. 2* (Eds.: N. Berova, P. L. Polavarapu, K. Nakanishi, R. W. Woody), Wiley, **2012**.
[43] a) S. Neidle, *Nat. Chem. Rev.* **2017**, *1*; b) B. Maji, S. Bhattacharya, *Chem. Commun.* **2014**, *50*, 6422–6438; c) G. W. Collie, G. N. Parkinson, *Chem. Soc. Rev.* **2011**, *40*, 5867–5892; d) S. Balasubramanian, S. Neidle, *Curr. Opin. Chem. Biol.* **2009**, *13*, 345–353.
[44] a) S. Asamitsu, T. Bando, H. Sugiyama, *Chem. Eur. J.* **2019**, *25*, 417–430; b) D. Monchaud, M. P. Teulade-Fichou, *Org. Biomol. Chem.* **2008**, *6*, 627–636.
[45] a) F. Caporaletti, J. Rubio-Magnieto, M. Lo, J. F. Longevial, C. Rose, S. Clément, A. van der Lee, M. Surin, S. Richeter, *J. Porphyrins Phthalocyanines* **2020**, *24*, 340–349; b) J. Rubio-Magnieto, S. Kajouj, F. Di Meo, M. Fosséprè, P. Trouillas, P. Norman, M. Linares, C. Moucheron, M. Surin, *Chem. Eur. J.* **2018**, *24*, 15577–15588; c) J. Rubio-Magnieto, F. Di Meo, M. Lo, C. Delcourt, S. Clément, P. Norman, S. Richeter, M. Linares, M. Surin, *Org. Biomol. Chem.* **2015**, *13*, 2453–2463.
[46] a) J. X. Dai, M. Carver, D. Z. Yang, *Biochimie* **2008**, *90*, 1172–1183; b) J. X. Dai, C. Punchihewa, A. Ambrus, D. Chen, R. A. Jones, D. Z. Yang, *Nucleic Acids Res.* **2007**, *35*, 2440–2450; c) A. Ambrus, D. Chen, J. X. Dai, T. Bialis, R. A. Jones, D. Z. Yang, *Nucleic Acids Res.* **2006**, *34*, 2723–2735.
[47] J. S. Hudson, L. Ding, V. Le, E. Lewis, D. Graves, *Biochemistry* **2014**, *53*, 3347–3356.
[48] D. Renciuk, J. Zhou, L. Beaurepaire, A. Guedin, A. Bourdoncle, J. L. Mergny, *Methods* **2012**, *57*, 122–128.
[49] a) G. N. Parkinson, F. Cuenca, S. Neidle, *J. Mol. Biol.* **2008**, *381*, 1145–1156; b) G. N. Parkinson, R. Ghosh, S. Neidle, *Biochemistry* **2007**, *46*, 2390–2397.
[50] a) W. Drozdz, A. Walczak, Y. Bessin, V. Gervais, X. Y. Cao, J. M. Lehn, S. Ulrich, A. R. Stefankiewicz, *Chem. Eur. J.* **2018**, *24*, 10802–10811; b) W.

Drożdż, Y. Bessin, V. Gervais, X.-Y. Cao, J.-M. Lehn, A. R. Stefankiewicz, S. Ulrich, *Chem. Eur. J.* **2018**, *24*, 1518–1521.
[51] A. Wolfe, G. H. Shimer, T. Meehan, *Biochemistry* **1987**, *26*, 6392–6396.
[52] a) E. Weyandt, G. M. ter Huurne, G. Vantomme, A. J. Markvoort, A. R. A. Palmans, E. W. Meijer, *J. Am. Chem. Soc.* **2020**, *142*, 6295–6303; b) D. J. van Dijken, P. Kovaricek, S. P. Ihrig, S. Hecht, *J. Am. Chem. Soc.* **2015**, *137*, 14982–14991.
[53] M. D. Hanwell, D. E. Curtis, D. C. Lonie, T. Vandermeersch, E. Zurek, G. R. Hutchison, *J. Cheminf.* **2012**, *4*.
[54] J. M. Wang, R. M. Wolf, J. W. Caldwell, P. A. Kollman, D. A. Case, *J. Comput. Chem.* **2004**, *25*, 1157–1174.
[55] N. M. Hassan, A. A. Alhossary, Y. G. Mu, C. K. Kwoh, *Sci. Rep.* **2017**, *7*.
[56] O. Trott, A. J. Olson, *J. Comput. Chem.* **2010**, *31*, 455–461.
[57] M. M. Jaghoori, B. Bleijlevens, S. D. Olabarriaga, *J. Comput.-Aided Mol. Des.* **2016**, *30*, 237–249.
[58] Delano, W. L. (2002). The PyMOL Molecular Graphics System. Available online at: https://ci.nii.ac.jp/naid/10020095229/en.
[59] see Figure S2 for protons assignment.

Manuscript received: October 28, 2020
Revised manuscript received: January 14, 2021
Accepted manuscript online: January 15, 2021